Geochimica et Cosmochimica Acta Vol. 50, pp. 1099–1115

0016-7037/86/$3.00 + .00

Lower crustal xenoliths from Queensland, Australia: Evidence for deep crustal assimilation and fractionation of continental basalts

R. L. RUDNICK, W. F. MCDONOUGH, M. T. MCCULLOCH and S. R. TAYLOR
Research School of Earth Sciences, The Australian National University, Canberra, A.C.T. 2601, Australia

(*Received August* 7, 1985; *accepted in revised form February* 26, 1986)

Abstract—A suite of mafic, granulite facies xenoliths from north Queensland possesses petrographic and geochemical features of basaltic cumulates crystallized at lower crustal pressures. Negative correlations between incompatible trace elements and Mg# and positive correlations between compatible trace elements and Mg# suggest the xenoliths are genetically related and crystallized from a continuously evolving melt. Zr, Hf, Y, HREE, Ti and V do not correlate with Mg#, but show excellent negative correlations with Al_2O_3 content, reflecting the proportion of cumulate plagioclase to clinopyroxene. These chemical trends also suggest the trace element concentrations have not been affected by subsolidus recrystallization. The xenoliths have a large range in Sr and Nd isotopic compositions ($^{87}Sr/^{86}Sr$ = 0.70239 to 0.71467, ϵ_{Nd} = +9.5 to −6.1) which cannot be produced by crystal fractionation alone, and excellent correlations between isotope ratios and Mg# suggest the variable isotope compositions are not due to mantle source heterogeneities.

These mafic xenoliths are proposed to be cumulate products from a melt undergoing simultaneous assimilation and fractional crystallization (AFC). The data illustrate that only a few percent AFC in lower crustal environments can dramatically change the Sr and Nd isotopic composition of a basaltic melt, and suggest the use of caution when inferring mantle source isotopic compositions from continental basalts. Additionally, the Nd isotopic data plot on a positive trend on an Sm-Nd isochron diagram with an age of ~570 Ma. However, if these xenoliths formed by AFC, the positive trend reflects mixing between two isotopic end members and has no age significance. The correlations between Sr and Nd isotopic compositions with Mg# degrade as the isotopic ratios are back-calculated to earlier times, suggesting the xenoliths are relatively young; the xenoliths may be related to the Cenozoic igneous activity which occurs throughout eastern Australia.

INTRODUCTION

INTEGRATED PETROGRAPHIC, geochemical and isotopic studies of lower crustal xenolith suites provide direct information on how and when portions of the lower crust formed. Moreover, xenoliths formed by cumulate processes can provide information on the origin and evolution of the melts from which they precipitate. We report the results of a combined petrographic, geochemical and isotopic study of mafic lower crustal xenoliths from north Queensland, Australia and show how trace element and isotopic analyses can be combined to define the dominant processes affecting lower crustal composition.

The xenoliths come from three Plio-Pleistocene (<2 Ma) alkali basalt vents in the Chudleigh volcanic province, north Queensland (STEPHENSON and GRIFFIN, 1976; STEPHENSON *et al.*, 1980): Batchelors Crater, Airstrip Crater and Sapphire Hill. These vents lie near the southern extension of the Burdekin fault zone, which is a steep, westward dipping thrust fault (WITHNALL, 1982) that separates Paleozoic volcanics and sediments of the Tasman fold belt on the east from Precambrian metamorphic rocks and granites of the Georgetown Inlier on the west (Fig. 1). The xenoliths are 5 to 50 cm in diameter; most with a blocky shape and coarse grain size (>2 mm) and all are mafic in composition ($SiO_2 \leqq 51\%$). There are three general classes of crustal xenoliths based on mineralogy and chemistry: (1) plagioclase-rich xenoliths, the most abundant type, (2) rarer, pyroxene-rich xenoliths and (3) xenoliths with mineralogy and major element compositions transitional between these two end members. The modal mineralogies and dominant textural features of the xenoliths are listed in Table 1 (petrographic descriptions are given in the Appendix). Here the xenoliths are grouped by mineralogy, with metamorphic grade increasing toward the bottom of the table. Because major element compositions of the plagioclase-rich xenoliths show little variation, their variable mineralogies are interpreted to reflect differing equilibration conditions. Hence, the olivine-bearing samples come from the shallowest levels and garnet, clinopyroxene-bearing samples come from the deepest levels (RUDNICK and TAYLOR, 1986). All of the xenoliths possess metamorphic textures, but relict cumulate textures (*i.e.*, orthopyroxene oikocrysts enclosing tabular plagioclase) are present in several of the plagioclase-rich samples. The xenolith mineral assemblages and cation exchange thermobarometry on coexisting mineral rims suggest equilibration conditions between 20–40 km and 700–1000°C (Fig. 2 and RUDNICK and TAYLOR, 1986). The presence of two coronal textures: (1) olivine rimmed by orthopyroxene and pyroxene-spinel symplectite and (2) spinel rimmed by garnets (Table 1), indicates these xenoliths crystallized at variable depths in the lower crust and cooled isobarically (KAY and KAY, 1983; RUDNICK and TAYLOR, 1986). Therefore, these xenoliths have not experienced a metamorphic "event", but rather, simply recrystallized to lower temperature mineralogies. Relict igneous textures are confined to the xenoliths which equili-

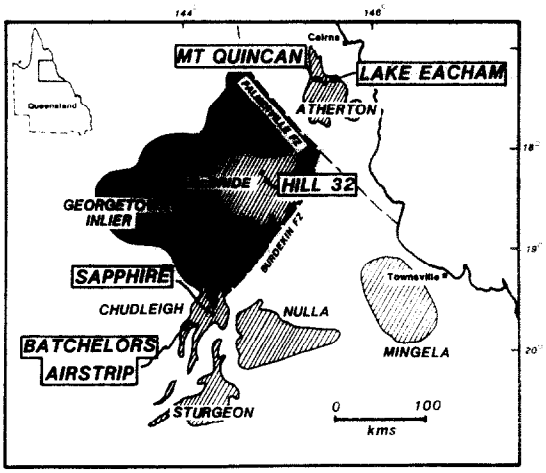

FIG. 1. Map of north Queensland Cenozoic volcanic provinces (hatched areas). Chudleigh province xenolith localities discussed here are Sapphire, Batchelors and Airstrip Craters. Shaded area is the Precambrian Georgetown Inlier, and the white areas to the east are Paleozoic volcanics, granites and sediments of the Tasman fold belt.

brated at the shallowest levels (Table 1). Deformation textures, present in some of the xenoliths (KAY and KAY, 1983; see Appendix), may reflect original igneous textures (*e.g.*, those in 83-107) or may have formed from reaction to localized stress fields associated with the nearby Burdekin fault zone.

Fourteen xenoliths were analyzed for major and trace elements; 11 of these were analyzed for their Sr and Nd isotopic compositions. The principal aims of this study were to (1) characterize the lower crust in this region of north Queensland; (2) identify the major lower crust-forming processes occurring there; (3) determine the age of this segment of lower crust; and (4) evaluate the significance of this data to continental magma evolution.

ANALYTICAL TECHNIQUES

Least altered xenoliths were chosen for chemical and isotopic analyses. The samples ranged from 260 to 1180 g, after removal of all weathered surfaces by sawing. The xenoliths were crushed in a steel jaw crusher, then the chips ground in an agate ring mill. No xenoliths showed invasion of the host basalt in thin section, although most suffered some decompression melting, manifested in kelyphite rims on the garnets (see KAY and KAY, 1983 and Appendix).

Major element analyses were obtained by wide-beam (15 kv) EDS microprobe analyses (REED and WARE, 1973) on glasses created in a positive Ar-pressure molybdenum strip heater. Each analysis represents the average of at least 10 spot analyses per sample. TiO_2 and P_2O_5 were measured for the same glasses using a Cameca, WDS, microprobe. Analytical uncertainty for all the major elements is less than 5%. V, Cr, Ni, Cu, Zn, Sr (and some Zr, Nb and Ba analyses—as indicated in Table 3) were obtained through XRF analyses (NORRISH and CHAPPELL, 1977). The remaining trace elements were measured *via* spark-source mass spectroscopy (TAYLOR and GORTON, 1977). Analytical uncertainty for most trace elements is less than 5%. Elements present in very low abun-

TABLE 1. Summary of Mineralogy and Textures in Chudleigh Province Xenoliths

Mineralogy	Samples	Textures
	Plagioclase-rich*	
Ol-Sp-Opx-Cpx-Pc	106 107 109	Relict igneous textures: poikilitic Px and lath-shaped Pc Coronas: Ol rimmed by Opx rimmed by Sp + Px. Pc composition: labradorite
Sp-Opx-Cpx-Pc	126 127 139 112	Relict igneous textures: large broken Pc? Coronas: Sp/Opx symplectites rimmed by Cpx. Pc comp: labradorite rimmed by andesine.
Sp-Gar-Opx-Cpx-Pc	114 131 138	Relict igneous textures: none? Coronas: Sp rimmed by Gar. Pc comp: labradorite or labradorite rimmed by andesine.
Gar-Opx-Cpx-Pc rare Sp cores	117 133 140	Relict igneous textures: none. Meta textures: polygonal crystals. Pc comp: andesine or labradorite rimmed by andesine.
Gar-Cpx-Pc rare Opx	125 BC	Relict Igneous Textues: none Meta textures: polygonal crystals; euhedral Gar. Pc comp: andesine.
	Pyroxene-rich	
Cpx-Opx-Pc-Rut±Ol	110 115	Relict igneous textures: possible cumulate layering. Meta. textures: polygonal Pc crystals. Pc comp.: labradorite.

Where Cpx = clinopyroxene, Opx = orthopyroxene, Ol = olivine, Pc = plagioclase, Sp = Spinel, Gar = garnet, Rut = rutile, Px = pyroxene.

*The two transitional xenoliths, 83-126 and BC, are grouped here with the plagioclase-rich xenoliths because of their high modal plagioclase content.

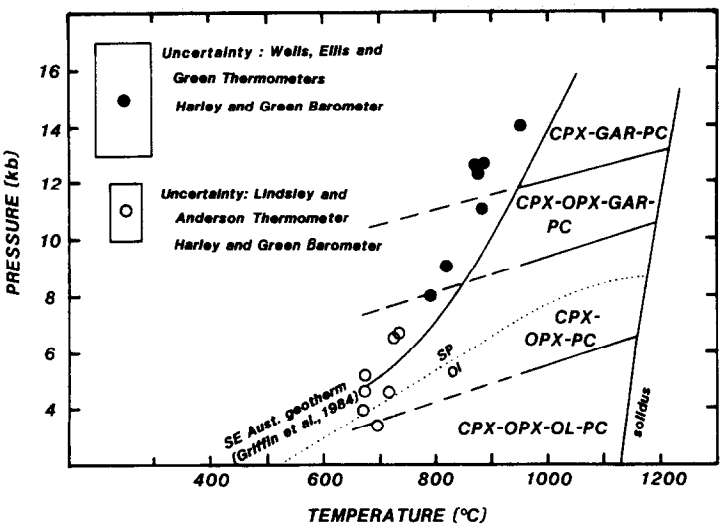

FIG. 2. Temperature and pressure estimates of garnet, two pyroxene plagioclase-rich xenoliths using the LINDSLEY and ANDERSON (1983) two pyroxene thermometer with the HARLEY and GREEN (1982) garnet-orthopyroxene barometer (open circles), or the WELLS (1977) two pyroxene or ELLIS and GREEN (1979) garnet-clinopyroxene thermometer with the HARLEY and GREEN (1982) barometer (closed circles). Points represent average of 5 analyses on adjacent mineral rims for each sample; boxes represent uncertainty. Experimentally determined stability fields are for a two pyroxene mafic xenolith from the Delegate breccia pipe which has major element composition similar to the Chudleigh plagioclase-rich xenoliths (IRVING, 1974). Dotted line represents spinel-olivine transition (HERZBERG, 1978). The plagioclase-rich xenoliths possess all the mineral assemblages shown here. Southeastern Australian geotherm of GRIFFIN *et al.* (1984) shown for reference.

dances, however, have higher uncertainties (10% for Th and U, 20% for Cs and Nb).

Dissolution procedures followed during this study are detailed in MCCULLOCH and CHAPPELL (1982). For each sample approximately 150 mg of powder was dissolved in teflon bombs. During the analyses of these samples the measured total chemical blank was 0.5 ng for Nd and 3.5 ng for Sr. No blank corrections were necessary for any of the isotope ratios. Mass spectrometry procedures and measured values for different isotopic standards are detailed in MCDONOUGH *et al.* (1985). Standard analyses performed concurrent with these analyses are listed at the bottom of Table 3.

RESULTS

Table 2 gives major element compositions and normative mineralogies for 10 plagioclase-rich, 2-pyroxene-rich and 2 transitional xenoliths. The plagioclase-rich xenoliths show little variation in SiO_2 (50 wt.%) and Al_2O_3 (20 wt.%), whereas Mg#s range from 41 to 76. Mg#s used here will be 100 (Mg/Mg + ΣFe), unless otherwise specified. Compared to the plagioclase-rich samples, the pyroxene-rich xenoliths have lower Al_2O_3 (9–10%), similar SiO_2 and higher Mg#s. Transitional xenoliths have major element compositions lying between the two end member types except that sample BC has the highest Mg# of the suite. All xenoliths are olivine-hypersthene normative, except plagioclase-rich xenolith 83-112, which has normative nepheline. This xenolith is also distinct from the rest of the plagioclase-rich xenoliths in that it is the only sample with large proportions of modal (and normative) ilmenite and magnetite, and because of this, it has the lowest Mg# of the suite.

Trace element concentrations are presented in Table 3. Chondrite normalized patterns (REE and Ba) are shown for the three xenolith types in Fig. 3. The plagioclase-rich xenoliths have low total REE concentrations (0.2 to 10 × chondrite), with LREE-enriched patterns and large positive Eu anomalies ($Eu/Eu^* = 1.5$ to 4.3). These patterns mimic the REE partition coefficients for plagioclase in equilibrium with mafic to intermediate liquids (SCHNETZLER and PHILPOTTS, 1970; IRVING, 1978; FUJIMAKI *et al.*, 1984). The pyroxene-rich xenoliths have LREE-depleted patterns, with no Eu anomalies and slight negatively sloped HREE (Fig. 3b). Such REE patterns are similar to REE partition coefficient patterns for clinopyroxene in equilibrium with mafic to intermediate liquids (SCHNETZLER and PHILPOTTS, 1970; IRVING, 1978; FUJIMAKI *et al.*, 1984). These xenoliths are unlikely to be crystallized basaltic liquids because of their low Na_2O and Al_2O_3 contents at relatively high SiO_2 content. The lack of a positive Eu anomaly in these samples suggests that plagioclase was not a cumulate or restite phase and the modal plagioclase formed either through subsolidus re-equilibration or through crystallization of interstitial melt. The transitional xenoliths (Fig. 3c) are LREE depleted, but possess a positive Eu anomaly, thus they have features transitional to those of the plagioclase-rich and pyroxene-rich xenoliths.

Trace elements which are highly incompatible in plagioclase, olivine and pyroxenes (the inferred original phases in these xenoliths) are present in low abundances and negatively correlate with Mg# (Fig. 4a). The correlation of K, Th and U with Mg# suggest these

TABLE 2. Major Element Chemistry and CIPW Normative Mineralogies[1] of Chudleigh Province Mafic Granulite Xenoliths

	Plagioclase-rich										Pyroxene-rich		Transitional	
	83-107 AC	83-112 AC	83-114 BC	83-117 BC	83-125 SH	83-127 SH	83-131 SH	83-133 SH	83-138 SH	83-140 SH	83-110 AC	83-115 BC	83-126 SH	BC BC
SiO_2	49.58	50.97	50.45	49.75	50.74	50.09	50.51	49.98	49.68	51.18	50.83	50.88	51.10	49.72
TiO_2	0.12	1.99	0.36	0.17	0.30	0.18	0.27	0.22	0.24	0.36	0.86	0.82	0.62	0.35
Al_2O_3	20.69	19.02	18.16	20.22	19.42	20.56	20.02	20.02	19.81	19.04	10.07	9.90	18.11	17.98
FeO*	8.27	10.11	7.66	6.48	6.85	7.03	6.80	7.93	6.96	8.78	10.54	7.32	6.10	5.00
MnO	0.12	0.14	0.16	0.09	0.12	0.11	0.12	0.13	0.14	0.18	0.22	0.19	0.13	0.11
MgO	9.38	3.95	9.58	11.79	9.85	10.26	9.61	10.06	10.37	8.24	16.30	14.38	8.81	11.62
CaO	9.06	8.66	10.62	8.74	10.66	8.55	10.15	8.90	9.97	8.84	9.75	15.64	12.04	12.57
Na_2O	3.03	4.92	2.80	2.55	2.48	2.71	2.82	2.65	2.59	3.12	1.05	0.88	2.98	2.51
K_2O	0.23	0.43	0.16	0.15	0.25	0.22	0.19	0.23	0.15	0.28	0.08	0.06	0.27	0.07
P_2O_5	0.07	0.18	0.05	0.04	0.06	0.06	0.06	0.07	0.10	0.11	0.17	0.05	0.07	0.15
TOTAL	100.55	100.37	100.00	99.98	100.73	99.77	100.55	100.19	100.01	100.13	99.87	100.02	100.26	100.08
Mg #[2]	66.9	41.0	69.0	76.4	71.9	72.2	71.6	69.3	72.9	62.6	73.4	77.8	72.0	80.5
q	0	0	0	0	0	0	0	0	0	0	0	0	0	0
c	0	0	0	0.07	0	0.46	0	0	0	0	0	0	0	0
or	1.36	2.54	0.95	0.89	1.48	1.30	1.12	1.36	0.89	1.65	0.47	0.35	1.60	0.41
ab	25.64	38.06	23.69	21.58	20.98	22.93	23.86	22.42	21.91	26.40	8.88	7.45	25.21	21.24
an	42.17	28.54	36.51	43.10	41.12	42.02	41.41	42.05	41.98	37.12	22.53	22.89	35.24	37.59
ne	0	1.93	0	0	0	0	0	0	0	0	0	0	0	0
di	1.88	11.04	12.81	0	9.16	0	6.89	1.33	5.49	4.90	19.86	42.96	19.32	19.50
hy	8.30	0	10.67	16.85	15.39	19.03	11.79	17.37	12.95	17.99	39.78	18.24	4.50	1.59
ol	19.34	12.26	13.21	15.93	10.68	12.30	13.61	13.67	14.85	9.56	4.44	5.26	11.91	17.83
mt	1.58	1.94	1.47	1.24	1.31	1.35	1.30	1.52	1.33	1.68	2.02	1.40	1.17	0.96
il	0.23	3.78	0.68	0.32	0.57	0.34	0.51	0.42	0.46	0.68	1.63	1.29	1.23	1.06
ap	0.17	0.43	0.12	0.09	0.14	0.14	0.14	0.17	0.20	0.26	0.40	0.33	0.17	0.09

FeO* = total Fe as Fe^{2+}; BC = Batchelor's Crater; AC = Airstrip Crater; SH = Sapphire Hill; [1]CIPW Norms calculated assuming $Fe_2O_3/FeO = 0.15$; [2]Mg # = 100 Mg/Mg + ΣFe

q = quartz, c = corundum, or = orthoclase, ab = albite, an = anorthite, ne = nepheline, di = diopside, hy = hypersthene, ol = olivine, mt = magnetite, il = ilmenite, ap = apatite

TABLE 3. Trace Element Chemistry of Chudleigh Province Mafic Granulite Xenoliths

	Plagioclase-rich										Pyroxene-rich		Transitional	
	83-107	83-112	83-114	83-117	83-125	83-127	83-131	83-133	83-138	83-140	83-110	83-115	83-126	BC
V	31	283	77	24	64	14	43	30	43	34	253	302	109	142
Cr	40	9	206	82	322	22	211	81	234	85	755	1070	680	419
Ni	159	34	133	155	86	159	123	118	164	58	228	282	106	345
Cu	39	44	38	24	25	29	43	25	33	7	35	49	24	25
Zn	59	78	55	44	49	52	45	54	48	75	73	42	46	25
Rb	0.63[2]	1.56[2]	0.56[2]	0.39	2.02[2]	0.85[2]	0.96[2]	2.0[1]	1.0[1]	1.97[2]	0.22[2]	0.45[2]	1.06[2]	0.59[2]
Sr	420	590	375	397	535	505	441	412	423	540	214	39[2]	409	350[2]
Y	1.25	5.74	6.70	1.63	4.54	1.22	2.65	3[1]	3[1]	3.94	17[1]	23[1]	8.25	11.0
Zr	2.9	70	12.9	3.5	8.0	4.9	8	--	--	10.1	28[1]	36[1]	15	16.9
Nb	0.73	1.77	0.72	0.62	0.73	0.91	0.67	0.5[1]	<0.5[1]	0.80	0.48	0.74	0.56	0.45
Cs	0.27	0.07	0.16	0.26	0.11	0.16	0.22			0.10	0.11	0.24	0.02	0.09
Ba	161	575[1]	180	52	120	305[1]	53	66[1]	56[1]	420[1]	19	25	83	12
La	2.61	4.21	2.39	1.74	2.03	2.12	2.34			3.23	1.11	2.04	2.22	1.32
Ce	3.05	8.84	4.40	2.58	4.36	4.36	3.92			6.44	4.43	6.07	7.80	2.73
Pr	0.40	1.14	0.63	0.32	0.59	0.52	0.50			0.86	0.67	1.12	1.03	0.54
Nd	1.60	5.71	3.36	1.50	3.00	2.18	2.45			4.17	4.33	7.20	5.50	3.50
Sm	0.26	1.65	1.00	0.32	0.84	0.36	0.62			1.06	1.70	2.70	1.62	1.31
Eu	0.79	1.91	0.88	0.36	0.58	0.52	0.56			1.71	0.65	0.94	0.80	0.65
Gd	0.23	1.78	0.93	0.29	0.97	0.27	0.65			1.07	2.17	3.44	1.72	1.58
Tb	0.03	0.28	0.14	0.04	0.17	0.04	0.12			0.19	n.d.	n.d.	0.29	0.29
Dy	0.24	1.46	1.00	0.34	1.12	n.d.	0.94			0.87	2.85	4.35	n.d.	2.10
Ho	0.05	0.28	0.23	0.08	0.22	0.03	0.15			0.21	0.61	0.93	0.35	0.46
Er	0.10	0.68	0.55	0.22	0.56	0.08	0.37			0.52	1.68	2.44	0.92	1.23
Yb	0.08	0.80	0.54	0.16	0.54	0.06	0.36			0.51	1.52	2.09	0.60	1.03
Hf	0.07	1.84	0.45	0.15	0.32	0.09	0.30			0.33	0.71	1.07	0.49	0.63
Pb	1.04	1.21	1.15	0.87	2.05	0.47	2.05			1.15	0.59	0.76	1.78	0.28
Th	--	0.15	0.03	0.02	0.07	0.04	0.07			0.11	0.03	0.04	0.10	0.03
U	--	0.13	0.02	--	0.02	0.02	0.02			0.05	--	0.01	0.03	0.01
W	0.43	0.54	0.17	0.20	0.25	0.20	0.27			0.46	--	0.28	0.10	0.34
Sn	0.59	0.80	0.58	0.44	0.55	0.32	0.55			0.48	0.98	1.32	0.55	0.65
Mo	0.29	0.41	0.15	0.15	0.16	0.10	0.17			0.20	0.34	0.53	0.12	0.23
$(La/Yb)_N$	22.0	5.7	3.0	7.2	2.5	23.0	4.4			4.3	0.5	0.66	2.5	0.87
$(La/Sm)_N$	6.3	1.6	1.5	3.2	1.5	3.7	2.4			1.9	0.4	0.5	0.9	0.6
(Eu/Eu^*)	4.2	3.4	2.9	3.8	2.0	5.1	2.8			4.9	1.0	1.0	1.5	1.3

[1]XRF values. [2]Isotope dilution values. -- means not detected. n.d. means not determined

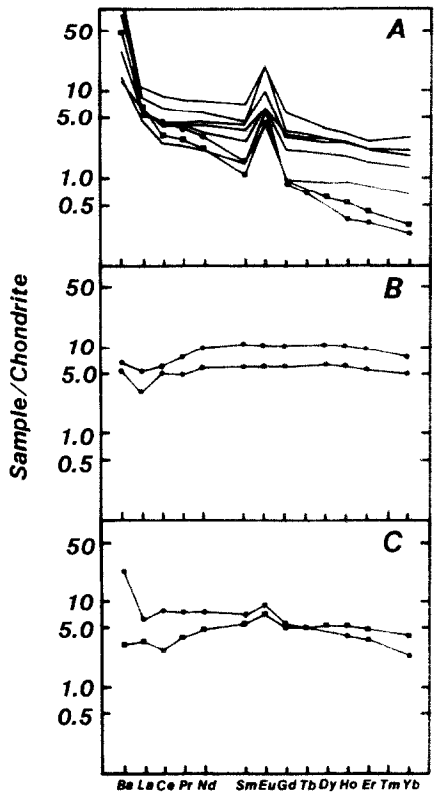

FIG. 3. Chondrite normalized REE and Ba concentrations for the three types of crustal xenoliths: (A) plagioclase-rich (pattern marked with squares is 83-107, pattern marked with circles is 83-127); (B) pyroxene-rich and (C) transitional xenoliths (pattern marked with squares is BC, pattern marked with circles is 83-126). Chondrite values from TAYLOR and MCLENNAN (1985).

elements have not suffered any depletion after crystallization in the deep crust. Compatible trace elements vary widely and positively correlate with Mg# (Fig. 4b).

Y, HREE, Zr, Hf, V and Ti are trace elements which, in basaltic systems, are moderately incompatible in clinopyroxene ($0.3 < D < 1.0$, where D = concentration of trace element in the crystal/concentration of element in the coexisting melt), but incompatible in plagioclase ($D < 0.05$ [IRVING, 1978; FUJIMAKI *et al.*, 1984]). These elements scatter when plotted against Mg#, but exhibit negative correlation with Al_2O_3 content (Fig. 5). (Note that 83-112 falls above the trends for V, Zr, Hf [and TiO_2], consistent with the presence of modal ilmenite and magnetite.) The size of the Eu anomaly (Eu/Eu*) exhibits a scattered, positive correlation with Al_2O_3. This suggests that these elements, and the Eu anomaly, are primarily controlled by the original proportions of pyroxene to plagioclase in the rocks. Sr, which is compatible in plagioclase (D = 1.0 to 2.5), less compatible in clinopyroxene (D = 0.1 to 0.2) and very incompatible in orthopyroxene and olivine ($D < 0.02$ [SCHNETZLER and PHILPOTTS, 1970; IRVING, 1978]), does not correlate with Al_2O_3, and produces a scattered, negative correlation with Mg# (Fig. 6a). Therefore, in the overall system Sr behaved incompatibly, and even though plagioclase-rich xenoliths form the majority of rock types in the suite, plagioclase was subordinate to ferromagnesian phases in the entire system. Rb shows a weak, negative correlation with Mg#, but exhibits a better correlation with Sr (Fig. 6b), suggesting that Rb has not been significantly affected by subsolidus recrystallization.

Table 4 presents Sr and Nd isotopic compositions for 10 of the xenoliths, chosen to span the range of chemical compositions present in the suite. In addition, $^{87}Sr/^{86}Sr$ ratios and ϵ_{Nd} for two of the host basalts are presented. $^{87}Sr/^{86}Sr$ ratios in the xenoliths vary widely from 0.70239 to 0.71467, and ϵ_{Nd} values range from +9.6 to −6.1. Most of the xenoliths plot along the mantle array, ranging from MORB-like values to values near bulk earth. Xenoliths with negative ϵ_{Nd} values fall to the right of the mantle array (Fig. 7). Except for sample 83-112, $^{87}Sr/^{86}Sr$ and ϵ_{Nd} correlate with Mg#, with correlation coefficients of −0.89 and 0.91, respectively (Fig. 8). For n = 11, this corresponds to a 99.99% level of significance.

The correlation between a wide variety of trace elements and isotopes with either Mg# or Al_2O_3 content indicates that these samples are genetically related, with the possible exception of 83-112. The petrologic, chemical and isotopic composition of sample 83-112 is distinct from the rest of the suite and implies a separate origin for this xenolith.

DISCUSSION

Significance of Mg# trends and trapped melt estimates

Before inferences about the xenoliths' origin can be made from the correlations between trace elements, isotopic ratios and Mg#, the principal parameters affecting the Mg# of the xenoliths must be delineated. Three parameters can affect Mg# in these xenoliths: (1) the original proportions of olivine, orthopyroxene and clinopyroxene, (2) the amount of trapped melt originally present, and (3) the composition of the coexisting melt (the term "coexisting melt" is used here as the melt with which the crystals were in contact with when they formed).

The large range in Mg#s is unlikely to be produced solely by varying the proportions of ferromagnesian minerals. The lowest whole-rock Mg# for the xenoliths is 63, and Mg# varies by 17 units for the entire suite (excluding 83-112, which has primary oxides). This variation is about twice that exhibited by coexisting olivines and pyroxenes in rocks with Mg#s > 60 from layered mafic intrusions (NWE, 1976; CAMPBELL, 1977; WILSON and LARSEN, 1985). Moreover, the concentrations of very incompatible trace elements (*e.g.*, U, Th, Ba, K, LREE) are not affected by the proportions of ferromagnesian phases. Thus the correlations between incompatible trace elements and Mg# (Fig. 4) suggests that factors other than phase proportions were important in establishing these trends.

Varying the proportions of trapped melt to ferromagnesian minerals could potentially yield the range

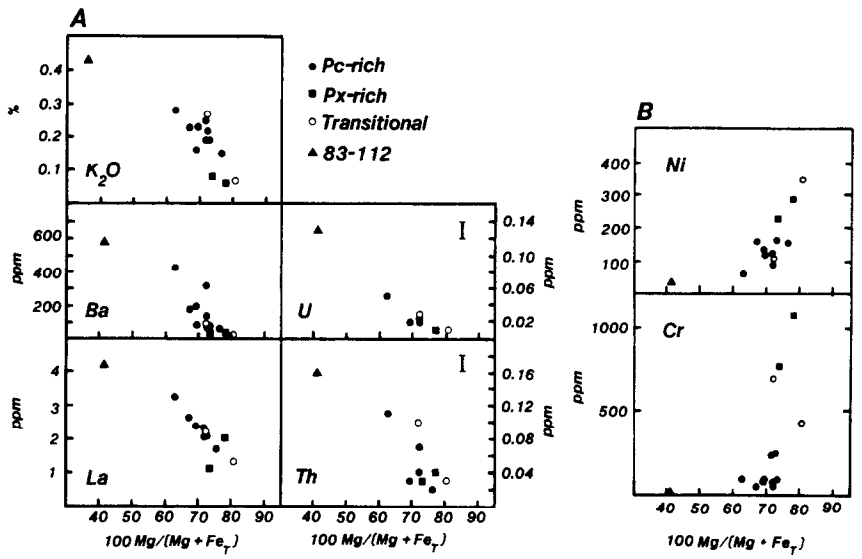

FIG. 4. (A) Incompatible trace elements plotted against Mg#. (B) Compatible trace elements plotted against Mg#. Symbols as in (A). Error bars provided for Th and U concentrations, uncertainties for other trace elements are close to the size of the data point. Pc = plagioclase, px = pyroxene.

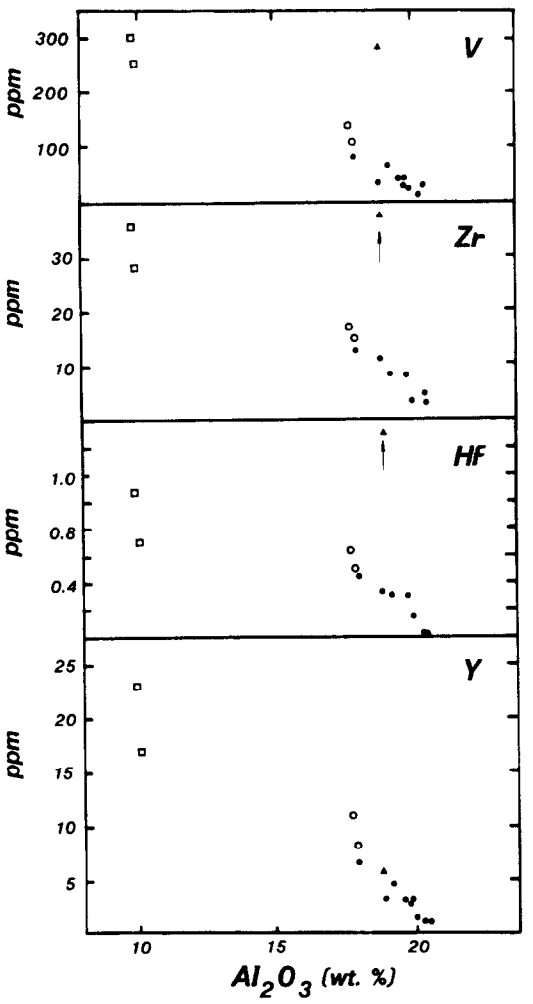

FIG. 5. V, Zr, Hf, Y plotted against Al_2O_3 content. TiO_2 and HREE show similar trends against Al_2O_3. Symbols as in Fig. 4. Note that 83-112 has elevated V, Zr and Hf, reflecting cumulate oxides.

of Mg#s and the correlations between Mg# and trace elements observed in the xenolith suite. However, if the trapped melt was in equilibrium with the crystals, the isotopic ratios would not change as a function of percentage of trapped liquid and the Mg#-isotope correlations could not be explained. Alternatively, the proportion of trapped melt could control the Mg#-isotope correlation if an evolved melt was percolated through the crystals (IRVINE, 1980; PALACZ and TAIT, 1985). In the Queensland xenoliths, metamorphic re-equilibration has completely obscured most igneous textures, so the proportion of trapped melt is not easily determined. However, the low incompatible trace element contents can be used to estimate the percentage of trapped melt in some samples. Sample 83-107 has one of the lower Mg#s of the suite (Mg# = 67). This sample also has extremely low HREE content (Yb < 0.4 times chondrite). If the trapped melt had a HREE content of 10 times chondrite (this is a minimum value since most eastern Australian basalts have higher HREE [FREY *et al.*, 1978; EWART, 1982; MCDONOUGH *et al.*, 1985]), only 4% trapped melt could have been present in this sample, if all of the HREE are contributed by the trapped melt. If half of the HREE are incorporated into the crystals, then only 2% trapped melt could have been present. This estimate is a maximum. Such a low proportion of trapped melt could not explain the low Mg#, higher incompatible trace element concentrations and more evolved isotopic compositions of this xenolith relative to the others.

The above observations suggest that the lower Mg#s in the xenoliths are not produced by greater proportions of trapped melt, but are primarily a function of the composition of the coexisting melt. That is, rocks with the lowest Mg# equilibrated with the most evolved melts, thus have the highest incompatible trace element concentrations, lowest compatible trace element concentrations and most radiogenic isotopic ratios.

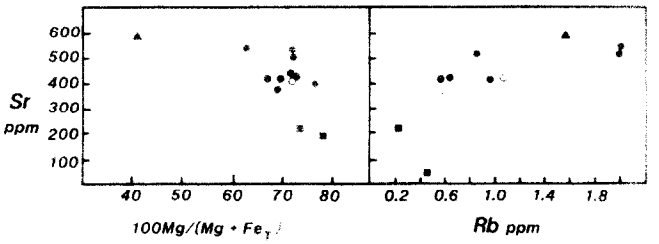

FIG. 6. (A) Sr plotted against Mg#. (B) Sr plotted against Rb. Symbols as in Fig. 4

Origin of the xenoliths: cumulate or restite?

The systematic chemical and isotopic variations observed in these xenoliths suggests a genetic relationship with one another. These features are consistent with the xenoliths forming as crystals in equilibrium with a continuously evolving melt or melts. This can occur in two possible scenarios: the xenoliths could represent either crystal cumulates from an evolving melt, or restite left behind after variable degrees of partial melt extraction. Distinguishing between a cumulate or restite origin is difficult, however, several criteria may be used.

(1) Most of the xenoliths have metamorphic textures, however, relict cumulate textures are preserved in samples derived from shallower levels (Table 1).

(2) Cumulates often have simple mineralogies due to the separation and accumulation of phases and adcumulus growth. In contrast, residua would be expected to have polymineralic assemblages, provided that degree of partial melting is not large. The pyroxene-rich xenoliths, which originally contained pyroxenes and olivine, would therefore fit a cumulate origin.

(3) Trace element concentrations will vary markedly between cumulates and residua (FREY and PRINZ, 1978). Small amounts of crystal fractionation will cause large variations in the concentrations of compatible trace elements (*e.g.*, Cr, Ni), since they are strongly partitioned into the crystallizing phases, causing their concentrations in the melt to decrease rapidly. In contrast, small amounts of fractional crystallization will not significantly change incompatible trace element (*e.g.*, La, U, Th, K and Rb) concentrations in the melt, and the corresponding cumulates will have low, and relatively uniform, concentrations of these elements. In the Queensland xenoliths, the very incompatible trace elements are present in low concentrations with a total variation of a factor of 4, whereas compatible trace elements have highly variable concentrations (Ni varies by a factor of 10, Cr varies by a factor of 100). This is consistent with the xenoliths forming as crystal cumulates rather than residua.

(4) The good correlations between Sr and Nd isotopic compositions and Mg# (Fig. 8) are not expected to result from variable degrees of partial melting of either a chemically and isotopically heterogeneous or homogeneous source region. The Mg# is a sensitive

TABLE 4. Isotopic Composition of Chudlegh Province Lower Crustal Xenoliths and Host Basalts

Sample	Rb	Sr	$^{87}Rb/^{86}Sr$	$^{87}Sr/^{86}Sr$	Sm	Nd	$^{147}Sm/^{144}Nd$	$^{143}Nd/^{144}Nd$	$\varepsilon_{Nd}(0)$	T(DM)	T(CHUR)
XENOLITHS											
Plagioclase-rich											
83-107	0.63	425.5	0.0042	0.71038 ± 3	0.31	1.59	0.1236	0.511621 ± 16	−11.2 ± 0.3	1.35	1.04
83-112	1.56	589.9	0.0076	0.70950 ± 5	1.66	6.17	0.1627	0.511798 ± 26	−0.8 ± 0.4	1.49	1.7
83-114	0.56	415.3	0.0039	0.70703 ± 6	1.10	3.59	0.1860	0.511707 ± 18	−2.5 ± 0.4	2500	1.83
83-125	2.02	548.6	0.0106	0.70446 ± 3	0.94	3.26	0.1752	0.511881 ± 20	+0.9 ± 0.4	1.43	1.4
83-127	0.85	516.6	0.0045	0.70468 ± 3	0.30	1.53	0.1201	0.511838 ± 32	0.0 ± 0.3	1.34	1.4
83-131	0.96	415.3	0.0059	0.70519 ± 3	0.62	2.26	0.1645	0.511794 ± 20	−0.8 ± 0.4	1.399	1.5
83-140	1.98	513.4	0.0111	0.71467 ± 5	0.89	3.53	0.1528	0.511525 ± 32	−6.1 ± 0.6	1.771	2.076
Pyroxene-rich											
83-110	0.22	214.7	0.0030	0.70410 ± 4	1.73	4.13	0.2541	0.512116 ± 36	−0.5 ± 0.7	1.7	1.7
83-115	0.45	39.3	0.0329	0.70473 ± 6	2.46	6.20	0.2396	0.511956 ± 18	−3.3 ± 0.3	1.9	1.9
Transitional											
83-126	1.06	422.5	0.0072	0.70473 ± 5	1.66	5.52	0.1823	0.511893 ± 38	−1.1 ± 0.7	1.64	1.7
BC	0.59	350.3	0.0048	0.70239 ± 3	1.29	3.38	0.2375	0.512326 ± 36	+9.6 ± 0.7	1.04	1.1
HOST BASALTS											
83-124	Batchelors Crater			0.70340 ± 5				0.512162 ± 16	+6.4 ± 0.3		
83-150	Sapphire Hill			0.70347 ± 5				0.512197 ± 20	+7.1 ± 0.4		

Elemental abundances are given in ppm and have analytical uncertainties of ≤ ± 0.5%. $^{87}Sr/^{86}Sr$ ratios were normalized to $^{86}Sr/^{88}Sr$ = 8.37520 and $^{143}Nd/^{144}Nd$ ratios were normalized to $^{146}Nd/^{142}Nd$ = 0.636151. Uncertainties in isotope ratios are 2σ_m and represent intra-run statistics. The mean measured $^{87}Sr/^{86}Sr$ ratio for E & A $SrCO_3$ is 0.70800 and for NBS-987 is 0.71022, with inter-run 2σ_m uncertainties of ≤ ± 0.00005. The mean measured $^{143}Nd/^{144}Nd$ ratios are 0.511833 for BCR-1, 0.511121 for Nd α and 0.511040 for the La Jolla Nd standard (cf., Wasserburg et al., 1981), with inter-run 2σ_m uncertainties of ≤ ± 0.000020.

Parameters used in ε_{Nd} and model age calculations: $(^{147}Sm/^{144}Nd)_{CHUR}$ = 0.1967, $(^{143}Nd/^{144}Nd)_{CHUR}$ = 0.512638, $(^{147}Sm/^{144}Nd)_{DM}$ = 0.225, $(^{143}Nd/^{144}Nd)_{DM}$ = 0.51235.

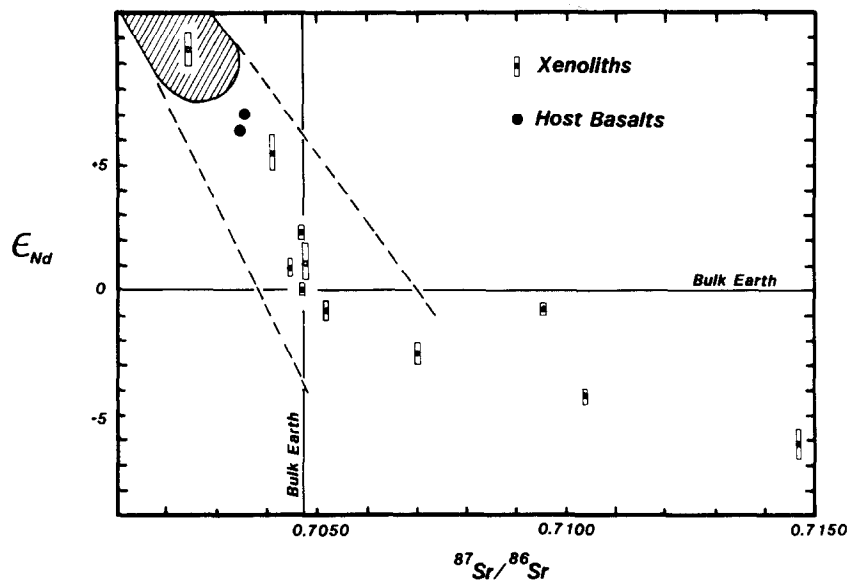

FIG. 7. Present day $^{87}Sr/^{86}Sr$ *versus* ϵ_{Nd} values for lower crustal xenoliths and host basalts. Symbols for xenoliths same as in Fig. 4. Hatched area is field of MORB. Dashed lines represent oceanic mantle array as defined by MORB and ocean island basalts, including St. Helena, Samoa, French Polynesia, Tristan da Cunha and Kerguelen (DEPAOLO and WASSERBURG, 1976; O'NIONS *et al.*, 1977; DOSSO and MURTHY, 1980; WHITE and HOFMANN, 1982; COHEN and O'NIONS, 1982).

indicator of the degree of partial melting, whereas Sr and Nd isotope ratios are insensitive to partial melting. Additionally, the Rb-Sr and Sm-Nd systems do not yield significant isochrons, thus suggesting the Mg#-isotope correlations reflect crystallization in an open system. Indeed, the range of $^{87}Sr/^{86}Sr$ ratios (0.7024 to 0.7147) is impossible to create through closed-system fractionation of a single melt. For example, if the xenoliths are derived from a melt with an initial $^{87}Sr/^{86}Sr$ ratio of 0.7024 (the lowest observed in the suite), then 83-140 (the sample with the highest $^{87}Sr/^{86}Sr$) would have initially needed 420 ppm Rb if it crystallized 300 Ma ago, or 62 ppm Rb if it crystallized 2500 Ma ago, in order to account for its high $^{87}Sr/^{86}Sr$ ratio. There are two major problems with this. First, if a plagioclase-rich cumulate like 83-140 has even 62 ppm Rb (a very high Rb content for a plagioclase cumulate, *cf.* MORSE, 1980), the Rb content of the coexisting liquid would be 520 to 1550 ppm Rb (using a bulk D_{Rb} = 0.04 to 0.12). These concentrations are unrealistically high. Secondly, this model would require the cumulate to have been depleted in Rb prior to or during entrainment in the host basalt. It is difficult to envision a Rb depletion which would preserve the correlation between Rb and Sr in the whole suite (Fig. 6b). Therefore, the high $^{87}Sr/^{86}Sr$ ratios observed in the more evolved rocks must be due to a process other than closed system crystal fractionation.

Given the xenoliths are cumulates, several observations rule against them being related to their host basalts. First, the $^{87}Sr/^{86}Sr$ ratios and ϵ_{Nd} value of the

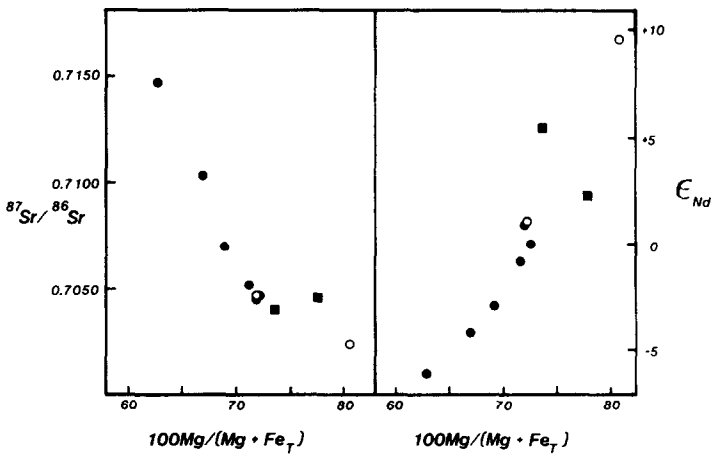

FIG. 8. $^{87}Sr/^{86}Sr$ and ϵ_{Nd} plotted against Mg#. 83-112, the one sample with primary Fe-oxides, is not plotted and would fall to the left of the diagrams. Symbols as in Fig. 4.

hosts are distinct from the isotopic compositions of the xenoliths (Table 4, Fig. 7). Secondly, as noted by FREY (1980) regarding the origin of Hawaiian pyroxenites, the ubiquitous metamorphic textures in these xenoliths suggest they are not direct cumulates from the host. Thirdly, the common occurrence of cumulate plagioclase in the xenoliths requires the coexisting liquid to have a negative Eu anomaly, yet the hosts have slight positive Eu anomalies (IRVING and FREY, 1984), as found in many other alkalic basalts (SUN and HANSON, 1975). Given these observations, it is concluded that the xenoliths are not precipitates from their host basalts.

Relative high $^{87}Sr/^{86}Sr$ ratios and low ϵ_{Nd} values are observed in some continental tholeiites and in some cases these features have been attributed to enriched mantle sources (MENZIES *et al.*, 1983; HAWKESWORTH *et al.*, 1983; KYLE *et al.*, 1983; MENZIES *et al.*, 1984; COX and HAWKESWORTH, 1985). Such an explanation for the range of $^{87}Sr/^{86}Sr$ ratios in the xenoliths is not consistent with the Mg#-isotope trends as it would require a very fortuitous relationship between the degree of melt fractionation and source composition.

AFC model

An alternative explanation for the observed trace element and isotopic correlations in the xenoliths is that the melt from which they crystallized was evolving through simultaneous assimilation and fractional crystallization (AFC). TAYLOR (1980), following BOWEN (1928), suggested that simple, two-component mixing is unlikely to describe the process of crustal assimilation because the heat required to melt crust must be derived from the latent heat of crystallization of the magma. Therefore, assimilation is likely to be accompanied by crystal fractionation and any assimilation models must include three components: magma, assimilate and cumulates. Most studies have applied AFC to explain compositional variations in lavas. The Queensland xenoliths provide an opportunity to examine the AFC process in mafic cumulates from the lower crust.

The isotopic and trace element variations produced through AFC can be described by a series of curves on isotope or trace element diagrams (TAYLOR, 1980; JAMES, 1981; DEPAOLO, 1981). The shape of the curves is primarily controlled by the elemental concentration ratios between the magma and assimilate and the chosen end member compositions. These curves reflect both melt and cumulate isotopic compositions at the time of crystallization, since cumulates will retain the isotope ratios of their coexisting melts. In the following arguments, we use Eqn. 15a of DEPAOLO (1981) to calculate the change in isotopic composition of the melt due to AFC. Both DEPAOLO (1981) and JAMES (1981) provide discussion of the effects of varying different input parameters on the shape of AFC curves.

The AFC model presented here is non-unique, given uncertainties in elemental concentrations and isotopic ratios in the parental melt and crustal assimilate(s). The following outlines the parameters chosen for our calculations and estimates of the uncertainty associated with each.

(1) r (the ratio of the mass of assimilate to the mass of crystals) is constant and equal to 0.85; such high values of r reflect the greater amount of assimilation possible in the warmer, lower crustal environment (JAMES, 1981). Changing r by 10% does not significantly change the shape of the curve but will move the position of the melt fraction. At higher r values the isotopic composition of the melt changes more dramatically at low percentages of AFC.

(2) the bulk D values ($\bar{D}$) are constant, with $\bar{D}_{Sr}$ = 0.8 (reflecting Sr's incompatible behavior in the entire system (Fig. 6a)) and $\bar{D}_{Nd} = 0.1$. Changing the bulk D values by factors of 2 does not significantly change the shapes of the curves;

(3) Sr and Nd concentrations in the parental magma are 550 and 20 ppm, respectively. These concentrations are similar to those for primitive tholeiitic and alkalic basalts from southern Queensland (EWART *et al.*, 1980; EWART, 1982) and western Victoria (FREY *et al.*, 1978; MCDONOUGH *et al.*, 1985).

(4) Sr and Nd concentrations in the assimilate are 200 and 30 ppm, respectively. These values represent average concentrations for felsic rocks of the Tasman Fold Belt (BLACK, 1980; MCCULLOCH and CHAPPELL, 1982; HENSEL *et al.*, 1985), which are likely candidates for the contaminant. Note that terrigenous sedimentary rocks will have similar Nd contents (*e.g.*, TAYLOR and MCLENNAN, 1985), but can have highly variable Sr contents (Sr = 23 to 287 ppm for eastern Australian shales and graywackes [BLACK, 1980; MCCULLOCH and CHAPPELL, 1982; EWART, 1982]).

(5) the isotopic composition of the parental magma is equal to that of the most primitive xenolith (BC).

(6) the isotopic ratios of the cumulates have not changed significantly since crystallization (*i.e.*, the xenoliths are younger than ~100 Ma; see below).

Given these assumptions, the isotopic composition of the assimilate can be varied to produce curves which mimic the isotope variations observed in the xenoliths. The Queensland xenoliths crystallized and cooled in the lower 20 km of the crust within the Tasman fold belt, therefore the abundant granites and sediments in this region are likely candidates for the assimilate. Present day $^{87}Sr/^{86}Sr$ for Tasman Fold Belt granites in north Queensland range from 0.7123 to 0.9110 (BLACK, 1980). In more southerly parts of the Tasman fold belt, granites have present day $^{87}Sr/^{86}Sr$ ranging from 0.7046 to 0.8417 and $^{143}Nd/^{144}Nd$ from 0.51109 to 0.51204 (MCCULLOCH and CHAPPELL, 1982; HENSEL *et al.*, 1985). The model assimilates used here fall near the middle of these large isotopic ranges.

Figure 9 presents three curves which correspond to different crustal end members; two curves bracket the data, the central curve represents an "average" model. Because the data do not lie along a single curve, it is likely that more than one crustal end member was in-

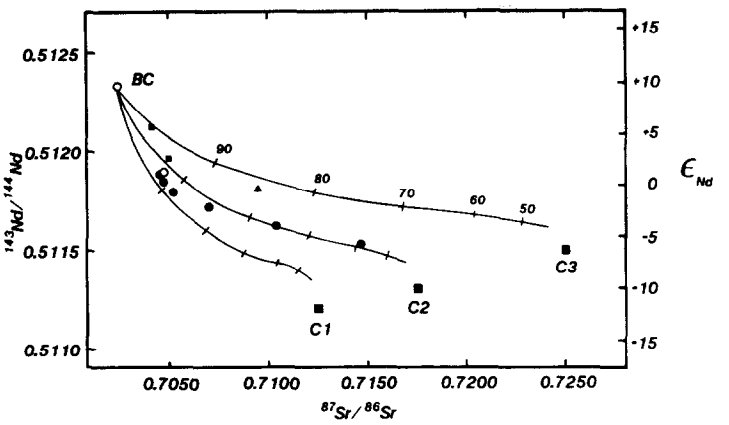

FIG. 9. AFC curves calculated using BC (the most primitive xenolith) as the starting composition and several crustal assimilates (C1, C2 and C3). Tick marks represent percentage of melt remaining.

volved. This is further supported by the range of depths from which the xenoliths were derived (20 to 40 km). In this context, it is interesting to note that there is a general correlation between depth of origin (as inferred from the mineralogies, Table 1) and isotopic composition: xenoliths derived from the deepest levels have more "primitive" isotopic ratios than xenoliths derived from shallow levels. However, this is not true for the most evolved sample (83-140), which is garnet-bearing. This may be evidence for more than one melt being involved.

The correlation between isotopic ratios and Mg# suggests a single isotopic composition for the parental melt. The mantle source region from which this melt was derived has the isotopic characteristics of MORB. However, this may not be true if the most primitive xenolith, BC, which is strongly LREE depleted, is actually older than the other xenoliths. Because BC falls along all the geochemical and isotopic trends, we consider it genetically related to the other xenoliths and thus include it in the model.

The $^{143}Nd/^{144}Nd$ ratio of the most evolved xenoliths can be used to place age constraints on the assimilate. Sample 83-107, the second most evolved xenolith, has a low $^{147}Sm/^{144}Nd$ ratio, thus is suitable for model age calculations (MCCULLOCH and WASSERBURG, 1978). This sample has a model age of 390 Ma, if derived from a chondritic mantle (Table 4). Because the isotopic composition of this xenolith is a mixture between the original magma and the assimilate, this age represents a minimum model age for the assimilate, *i.e.*, the crustal assimilate must have been derived from the mantle before 390 Ma. The model age of the assimilate could be much older than this if 83-107 contains only a small proportion of assimilate and/or the assimilate was derived from a depleted mantle (T_{DM} = 1000 Ma; Table 4).

Nature of the coexisting liquid

The trace element and isotopic correlations exhibited by the xenoliths suggest they represent crystals that accumulated within the lower crust from a single melt or a series of related melts, which evolved through assimilation and fractional crystallization. The bulk composition of the coexisting melt is difficult to estimate accurately without knowing the proportion of cumulates to liquid in the system. Nevertheless, several indirect methods can be used to estimate bulk composition. First, given the limited amount of trapped melt originally present, the normative mineralogies of the xenoliths may be taken as a guide to the original cumulate phases (*cf.* ROGERS and HAWKESWORTH, 1982). The presence of olivine and Ca-rich plagioclase in the norms suggest the xenoliths crystallized from a mafic melt. Secondly, the Mg# of modal olivine can be used to calculate the Mg# of the coexisting liquid, assuming $D^{ol/melt}_{Fe/Mg}$ = 0.3 (ROEDER and EMSLIE, 1970). Modal olivine is present in one of the analyzed samples (83-107), but is variably altered to iddingsite (see Appendix). Probe analyses for these olivines show that Fo contents negatively correlate with Al_2O_3 contents, consistent with a lowering of Fo content due to alteration (DEER *et al.*, 1982). The least altered olivines in this sample are Fo_{70} (with 0.33% Al_2O_3). If this is taken as an approximation of the igneous olivine's composition, then the coexisting melt had an Mg# of 41, using total Fe as $Fe+^2$. If one assumes an $Fe+^3/Fe+^2$ ratio of 0.15, then the coexisting melt had Mg# = 45. Sample 83-107 has one of the lower Mg#s of the suite, so this Mg# represents a lower estimate for the associated melts. This is consistent with the coexisting melt(s) being basaltic, with Mg#s generally >40.

Implications for continental lavas

In the AFC model presented above, the most contaminated xenolith is produced through 40% crystallization of the melt. If this melt were erupted, it would have chemical and Sr and Nd isotopic characteristics similar to those of other evolved continental basalts (*i.e.*, Mg# $\approx$ 40, negative Eu anomaly, low ϵ_{Nd} and high $^{87}Sr/^{86}Sr$). Unless the magma was tapped after only a few percent fractionation, the isotopically

MORB-like mantle source region for the xenolith's parental magmas would never be recognized. This illustrates the difficulty in inferring mantle compositional variations from continental lavas which have undergone any differentiation within the lower crust.

Oxygen isotopes are often used to delineate the amount of crustal assimilation that has occurred in basaltic melts, yet little is known about the effects of granulite facies metamorphism on $\delta^{18}O$ values. Some granulites exhibit slight decreases in $\delta^{18}O$ relative to their unmetamorphosed precursors (JAMES *et al.*, 1980; VALLEY and O'NEIL, 1984), whereas others exhibit significant $\delta^{18}O$ depletions as a result of metamorphism (SHIEH and SCHWARCZ, 1974; WILSON and BAKSI, 1983). Thus it is difficult to generalize about the $\delta^{18}O$ values of felsic granulites, which could be an important contaminant of basaltic magma in the lower crust. Preliminary oxygen isotope measurements of the Queensland xenoliths reveal that the most evolved xenolith in this suite (83-140) has a $\delta^{18}O$ value of +5.7‰ (RUDNICK and CHIVAS, unpubl. data). Oxygen isotopes will not be significantly fractionated during igneous crystallization. Therefore, if the oxygen isotopes of this rock have not exchanged with an external reservoir during isobaric cooling and development of the metamorphic mineralogy, then this $\delta^{18}O$ value reflects that of the coexisting melt. This, in turn, suggests that the assimilate may have had very low $\delta^{18}O$ yet high $^{87}Sr/^{86}Sr$ and low ϵ_{Nd}.

Age of the lower crust

The Queensland xenoliths plot along a scattered, positive trend on an $^{147}Sm/^{144}Nd$ *versus* $^{143}Nd/^{144}Nd$ isochron diagram (Fig. 10). If all the data points are considered, the regression yields an age of 570 ± 370 Ma with an initial $^{143}Nd/^{144}Nd$ ratio of 0.51118 ± 45 (ϵ_{Nd} = +1.6) (using the model 4 regression technique of MCINTYRE *et al.*, 1966). However, if the above model of AFC is correct, then a positive trend would be produced on this diagram due to mixing between melt and assimilate. Since the xenoliths are cumulates, they would not be expected to plot along a straight mixing curve because their $^{147}Sm/^{144}Nd$ ratio is a function of both melt and assimilate compositions and cumulate mineralogy, whereas the $^{143}Nd/^{144}Nd$ ratio is a function of assimilation only. For example, assimilation will cause the data to fall along a line joining the original melt to the assimilate. Superimposed upon this are the effects of crystal accumulation. Pyroxene-rich xenoliths with LREE depletions will fall to the right of the mixing line, whereas LREE-enriched plagioclase-rich xenoliths will fall to the left of the mixing line (Fig. 10, inset). This explains the observed scatter in Fig. 10, and suggests that the positive trend is due to mixing between two end members and has no age significance.

The Queensland xenoliths possess geochemical features indicative of a common origin, and do not show the effects of element depletion often associated with granulite facies metamorphism. Yet for these xenoliths it is probably misleading to attach any age significance to the positive slope in Fig. 10. So is there any age information available from these data? The cumulate process creates highly variable whole rock Sm/Nd ratios, but generally very low Rb/Sr ratios. Consequently, the present $^{87}Sr/^{86}Sr$ ratios in the xenoliths are likely to reflect their initial values, whereas the $^{143}Nd/^{144}Nd$ ratios will change dramatically with time. The present correlation between ϵ_{Nd} and $^{87}Sr/^{86}Sr$ for the Queensland xenoliths becomes progressively weaker as the isotope ratios are back-calculated to earlier times. In addition, the good correlation of isotope ratios with

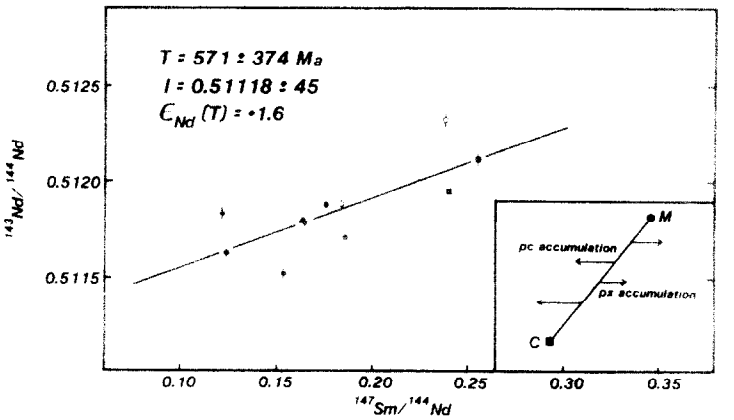

FIG. 10. Sm-Nd isochron diagram for lower crustal xenolith suite. Line represents regression yielding age of 571 ± 374 Ma. Symbols as in Fig. 4. Inset: schematic drawing showing predicted $^{143}Nd/^{144}Nd$ and $^{147}Sm/^{144}Nd$ ratios for cumulates derived from melt (M) which is mixing with assimilate (C). Note that the line in the inset is not meant to coincide with the regression line shown in the main figure. It is assumed that the $^{147}Sm/^{144}Nd$ ratio of (M) is less than or equal to 0.197, in order to have a chondritic or LREE enriched melt. Accumulation of plagioclase (pc) causes $^{147}Sm/^{144}Nd$ to decrease, whereas accumulation of pyroxene (px) causes $^{147}Sm/^{144}Nd$ to increase relative to the melt. The melt composition continuously evolves between M and C

Mg# (Fig. 8) becomes more scattered in the past. The correlation coefficient (r) for present day ϵ_{Nd} values *versus* Mg# is 0.91, at 400 Ma, $r = 0.79$ and at 1000 Ma, $r = -0.01$. Therefore, if we assume that the correlation of ϵ_{Nd} with Mg# is, like the trace element-Mg# correlations, due to AFC processes, then the time at which the greatest correlation exists may give the most reasonable age for the suite. This suggests the xenolith suite is relatively young (<100 Ma); and is probably not Paleozoic, as implied by the pseudoisochron.

Before any useful age information can be obtained from a suite of metamorphic rocks, it must first be shown that the rocks are genetically related (with the same initial ratio) and that their isotope ratios have not been affected by metamorphism. With a xenolith suite these problems are magnified due to lack of any field relationships. In addition, many investigators have plotted felsic xenoliths on the same isochrons as mafic xenoliths (ROGERS and HAWKESWORTH, 1982; MCCULLOCH *et al.*, 1982), but have not attempted to provide chemical evidence for their proposed genetic link.

If AFC was operating during the generation of other xenolith suites, it may be detectable by back-calculating isotope ratios to see if they lie along an AFC-type mixing curve at any time in the past. For example, the range of $^{87}Sr/^{86}Sr$ ratios present in Calcutteroo xenoliths from South Australia (MCCULLOCH *et al.*, 1982) suggests AFC may have been important in their evolution. Present day isotope ratios for the mafic xenoliths show considerable scatter on an ϵ_{Nd} *vs.* $^{87}Sr/^{86}Sr$ diagram (Fig. 11a). However, a linear trend is obtained at 1300 Ma (Fig. 11b). Figure 11 also shows the north Queensland data at present (c) and at the pseudoisochron age of 570 Ma (d) for comparison. By analogy with the Queensland xenoliths, the 2.5 Ga age reported by MCCULLOCH *et al.* (1982) for the Calcutteroo xenoliths may be an artifact produced by mixing of 1300 Ma mafic magma with older silicic crust. Of course, there are large uncertainties associated with these ages, and factors such as whether the rocks are originally cogenetic or have undergone post-crystallization Rb depletion, will add to the uncertainty. Other mafic xenolith suites for which isochrons have been published either do not show high $^{87}Sr/^{86}Sr$ ratios (*i.e.*, Lesotho xenoliths), or do not back-calculate to linear trends in the past (Eifel xenoliths, STOSCH *et al.*, 1986). Therefore, this model may be applicable in only some cases and each xenolith suite clearly needs to be evaluated separately.

Composition of the lower crust

The majority of granulite facies xenoliths from eastern Australian volcanic pipes are mafic and probably represent basaltic melts with variable proportions of cumulate phases (EDWARDS *et al.*, 1979; WILKINSON and TAYLOR, 1980; KAY and KAY, 1983; WASS and HOLLIS, 1983; ARCULUS *et al.*, 1986; GRIFFIN and O'REILLY, 1986; RUDNICK and TAYLOR, 1986). Seismic refraction profiles across the Tasman fold belt in southern Queensland and New South Wales show a high velocity lower crust (V_p = 6.7 to 7.7 km/sec, FINLAYSON, 1982; FINLAYSON *et al.*, 1984), indicative of a mafic composition.

The data for the Queensland xenoliths presented here may be used to clarify when and how the lower crust formed. If the Queensland xenoliths are Cenozoic cumulates associated with intrusion of basaltic magmas into the lower crust, then they significantly postdate

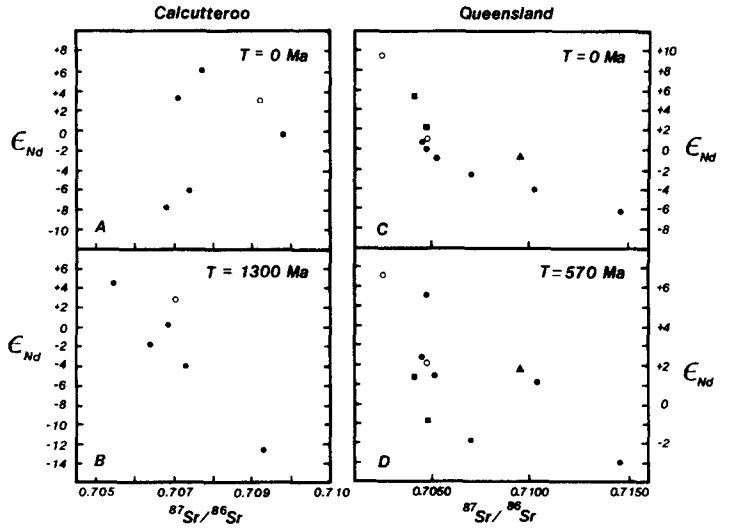

FIG. 11. (A) Present day $^{87}Sr/^{86}Sr$ *versus* ϵ_{Nd} values for mafic Calcutteroo xenoliths from south Australia (MCCULLOCH *et al.*, 1982). Filled circles are mafic granulites; open circle is an eclogite. (B) $^{87}Sr/^{86}Sr$ *versus* ϵ_{Nd} for Calcutteroo xenoliths at 1300 Ma. (C) Present day $^{87}Sr/^{86}Sr$ *versus* ϵ_{Nd} for Chudleigh province xenoliths compared with ratios for same xenoliths at 570 Ma (D) (pseudoisochron age). Symbols as in Fig. 4.

the sediments, lavas and granites of the Paleozoic Tasman fold belt. The observation that the parental magma to the xenoliths was affected by assimilation of isotopically evolved crustal material suggests the existence of felsic to intermediate rocks in the lower crust at the time of magma intrusion. Basaltic magmas ranging from highly silica undersaturated to saturated compositions have erupted in the highlands of eastern Australia from 70 Ma to Recent times (WELLMAN and MCDOUGALL, 1974). Of the three types of igneous provinces identified by WELLMAN and MCDOUGALL (1974), basalts of the central volcano provinces have been associated with deep crustal fractionation (EWART *et al.*, 1980; EWART, 1982; KNUTSON *et al.*, 1986) and extensive basaltic underplating is predicted to attend their formation (EWART *et al.*, 1980).

The eastern Australian central volcano provinces show a progressive decrease in age from north to south, which has been interpreted as a hot-spot trace (WELLMAN and MCDOUGALL, 1974; SUTHERLAND, 1983). The northernmost central volcano province is 32–33 Ma old and lies at 21° South. This is about 400 km east and 60 km south of the vents in the Chudleigh province. Assuming volcano spacing is regulated by the tensional stress field along the highlands (STEPHENSON and LAMBECK, 1985) and a migration rate of 66 km/Ma (WELLMAN and MCDOUGALL, 1974) for the central volcano-type activity, the hot spot would be predicted to be within the Chudleigh region some 33–35 Ma ago. A 35 Ma crystallization age is consistent with the chemical and isotopic data, thus the xenoliths may represent a lower crustal manifestation of basaltic magmatism in the region. Consequently, the Cenozoic igneous activity throughout eastern Australia may have provided more volumetrically significant crustal additions than are represented by the extruded rocks alone.

CONCLUSIONS

Integrated petrographic, geochemial and isotopic data for the granulite facies xenoliths from north Queensland indicate the rocks formed as cumulates from an evolving continental tholeiitic or alkalic basaltic magma which crystallized deep within the crust and isobarically re-equilibrated. The coherent geochemical and isotopic trends suggest that the basaltic liquid evolved through simultaneous crystal fractionation and assimilation of felsic crustal material. In particular, the good correlation between Sr and Nd isotopic composition and Mg# rule out mantle source heterogeneities as a means of producing the observed spread in isotopic compositions and suggests a young (Cenozoic) age for these xenoliths. The inferred isotopic composition of the mantle source region for this suite has a long term LREE and Rb depleted character, similar to the MORB source region. Features of this study which have wide ranging implications are:

(1) The enriched isotope compositions for these xenoliths are produced through simultaneous assimilation and fractionation, suggesting the use of caution when interpreting mantle source characteristics from continental tholeiites which have experienced even limited amounts of fractionation within the lower crust;

(2) The positive correlation between $^{147}Sm/^{144}Nd$ and $^{143}Nd/^{144}Nd$ is a product of mixing of a basaltic magma and an older, felsic crustal component and has no age significance. Thus, careful evaluation of trace element data along with isotopic results is required to interpret the meaning of possible "isochrons" from lower crustal xenolith suites.

(3) It may be possible to determine the age of genetically related lower crustal xenolith suites that have evolved through AFC-type processes by back-calculating their isotopic ratios to the time at which the samples plot along a trend on an ϵ_{Nd} *versus* $^{87}Sr/^{86}Sr$ diagram.

(4) These xenoliths provide evidence for Cenozoic basaltic underplating in the lower crust of eastern Australia, though the volumetric significance of this process is not constrained.

Acknowledgements—We thank Bruce Chappell for trace element XRF analyses and Allan Chivas for the oxygen isotope measurement. Useful discussions with Allan Chivas on oxygen isotopes, Shen-su Sun on trace elements and Herb McQueen and Russell Shaw on eastern Australian geology helped us develop some of the models presented here. We thank Drs. L. P. Black, W. L. Griffin, S. M. Kay, M. A. Menzies, S. Y. O'Reilly, H-G. Stosch and G. Wörner who contributed very useful critical comments on earlier versions of this paper. We thank Mike Shelley for assistance with the AFC computer program. RLR was partially supported through an NSF graduate fellowship. RLR and WFM were supported by ANU Ph.D. scholarships.

Editorial handling: F. A. Frey

REFERENCES

ARCULUS R. J., FERGUSON J., CHAPPELL B. W., SMITH D., MCCULLOCH M. T., JACKSON I., HENSEL H. D., TAYLOR S. R., KNUTSON J. and GUST D. A. (1986) Eclogites and granulites in the lower continental crust: examples from eastern Australia and southwestern U.S.A. In *Eclogites and Related Rocks* (ed. D. C. SMITH). Elsevier (in press).

BLACK L. P. (1980) Rb-Sr systematics of the Claret Creek Ring Complex and their bearing on the origin of Upper Palaeozoic igneous rocks in northeast Queensland. *J. Geol. Soc. Australia* **27**, 157–166.

BOWEN N. L. (1928) *The Evolution of the Igneous Rocks*. Dover, New York, N.Y., 1956 reprint of 1928 ed. Univ. Press, 332p.

CAMPBELL I. H. (1977) A study of macro-rhythmic layering and cumulate processes in the Jimberlana intrusion, Western Australia. Part I: the upper layered series. *J. Petrol.* **18**, 83–215.

COHEN R. S. and O'NIONS R. K. (1982) Identification of recycled continental material in the mantle from Sr, Nd and Pb isotope investigations. *Earth Planet. Sci. Lett.* **61**, 73–84.

COX K. G. and HAWKESWORTH C. J. (1985) Geochemical stratigraphy of the Deccan Traps at Mahabaleshwar, western Ghats, India, with implications for open system magmatic processes. *J. Petrol.* **26**, 355–377.

DEER W. A., HOWIE R. A. and ZUSSMAN J. (1982) *Orthosilicates* (second edition). Longman, London, 919p.

DEPAOLO D. J. (1981) Trace element and isotopic effects of combined wallrock assimilation and fractional crystallization. *Earth Planet. Sci. Lett.* **53**, 189–202.

DEPAOLO D. J. and WASSERBURG G. J. (1976) Inferences about magma sources and mantle structure from variations of $^{143}Nd/^{144}Nd$. *Geophys. Res. Lett.* **3**, 743–746.

DOSSO L. and MURTHY V. R. (1980) A Nd isotopic study of the Kerguelen islands: inferences on enriched oceanic mantle sources. *Earth Planet. Sci. Lett.* **48**, 268–276.

EDWARDS A. C., LOVERING J. F. and FERGUSON J. (1979) High pressure basic inclusions from the Kayrunnera kimberlitic diatreme in New South Wales, Australia. *Contrib. Mineral. Petrol.* **69**, 185–192.

ELLIS D. J. and GREEN D. H. (1979) An experimental study of the effect of Ca upon garnet-clinopyroxene Fe-Mg exchange equilibria. *Contrib. Mineral. Petrol.* **71**, 13–22.

EWART A. (1982) Petrogenesis of the Tertiary anorogenic volcanic series of southern Queensland, Australia, in light of trace element geochemistry and O, Sr and Pb isotopes. *J. Petrol.* **23**, 344–382.

EWART A., BAXTER K. and ROSS J. A. (1980) The petrology and petrogenesis of the Tertiary anorogenic mafic lavas of southern and central Queensland, Australia—possible implications for crustal thickening. *Contrib. Mineral. Petrol.* **75**, 129–152.

FINLAYSON D. M. (1982) Geophysical differences in the lithosphere between Phanerozoic and Precambrian Australia. *Tectonophys.* **84**, 287–312.

FINLAYSON D. M., COLLINS C. D. N. and LOCK J. (1984) P-wave velocity features of the lithosphere under the Eromanga Basin, eastern Australia, including a prominent mid-crustal (Conrad?) discontinuity. *Tectonophys.* **101**, 267–291.

FREY F. A. (1980) The origin of pyroxenites and garnet pyroxenites from Salt Lake Crater, Oahu, Hawaii: trace element evidence. *Amer. J. Sci.* **280A**, 427–449.

FREY F. A. and PRINZ M. (1978) Ultramafic inclusions from San Carlos, Arizona: petrologic and geochemical data bearing on their petrogenesis. *Earth Planet. Sci. Lett.* **38**, 129–176.

FREY F. A., GREEN D. H. and ROY S. (1978) Integrated models of basalt petrogenesis: a study of quartz tholeiites to olivine melilitites from south eastern Australia utilizing geochemical and experimental petrological data. *J. Petrol.* **19**, 463–513.

FUJIMAKI H., TATSUMOTO M. and AOKI K-I. (1984) Partition coefficients of Hf, Zr, and REE between phenocrysts and groundmasses. *Proc. Lunar Planet. Sci. Conf. 14th*, Part 2; *J. Geophys. Res.* **89**, B662–B672.

GRIFFIN W. L., WASS S. Y. and HOLLIS J. D. (1984) Ultramafic xenoliths from Bullenmerri and Gnotuk Maars, Victoria, Australia: petrology of a subcontinental crust-mantle transition. *J. Petrol.* **25**, 53–87.

GRIFFIN W. L. and O'REILLY S. Y. (1986) The lower crust in eastern Australia. *J. Geol. Soc. Lond.* (in press).

HARLEY S. L. and GREEN D. H. (1982) Garnet-orthopyroxene barometry for granulites and peridotites. *Nature* **300**, 697–701.

HAWKESWORTH C. J., ERLANK A. J., MARSH J. S., MENZIES M. A. and VAN CALSTEREN P. (1983) Evolution of the continental lithosphere: evidence from volcanics and xenoliths in southern Africa. In *Continental Basalts and Mantle Xenoliths* (eds. C. J. HAWKESWORTH and M. J. NORRY), pp. 111–138. Shiva Pub. Ltd., Cheshire, U.K.

HENSEL H.-D., MCCULLOCH M. T. and CHAPPELL B. W. (1985) The New England Batholith: constraints on its derivation from Nd and Sr isotopic studies of granitioids and country rocks. *Geochim. Cosmochim. Acta* **49**, 369–384.

HERZBERG C. T. (1978) Pyroxene geothermometry and geobarometry: exerimental and thermodynamic evaluation of some subsolidus phase relations involving pyroxenes in the system CaO-MgO-Al_2O_3-SiO_2. *Geochim. Cosmochim. Acta* **42**, 945–957.

IRVINE T. N. (1980) Magmatic infiltration metasomatism, double-diffusive fractional crystallization, and adcumulus growth in the Muskox intrusion and other layered intrusions. In *Physics of Magmatic Processes* (ed. R. B. HARGRAVES), pp. 325–383. Princeton Univ. Press.

IRVING A. J. (1974) Geochemical and high pressure experimental studies of garnet pyroxenite and pyroxene granulite xenoliths from the Delegate basaltic pipes, Australia. *J. Petrol.* **15**, 1–40.

IRVING A. J. (1978) A review of experimental studies of crystal/liquid trace element partitioning. *Geochim. Cosmochim. Acta* **42**, 743–770.

IRVING A. J. and FREY F. A. (1984) Trace element abundances in megacrysts and their host basalts: constraints on partition coefficients and megacryst genesis. *Geochim. Cosmochim. Acta* **48**, 1201–1221.

JAMES D. E. (1981) The combined use of oxygen and radiogenic isotopes as indicators of crustal contamination. *Ann. Rev. Earth Planet. Sci.* **9**, 311–344.

JAMES D. E., PADOVANI E. R. and HART S. R. (1980) Preliminary results on the oxygen isotopic composition of the lower crust, Kilbourne Hole, New Mexico. *Geophys. Res. Lett.* **7**, 321–324.

KAY S. M. and KAY R. W. (1983) Thermal history of the deep crust inferred from granulite xenoliths, Queensland, Australia. *Amer. J. Soc.* **283-A**, 486–513.

KNUTSON J., MCDONOUGH W. F., DUGGAN M. B. and CHAPPELL B. W. (1986) Geochemical and isotopic characteristics of eastern Australian Cainozoic "central" volcanoes. (abstr.) *Internat. Volc. Congress*, p. 174.

KYLE P. R., PANKHURST R. J. and BOWMAN J. R. (1983) Isotopic and chemical variations in Kirkpatrick basalt gorup rocks from south Victoria Land. In *Antarctic Earth Science* (eds. R. L. OLIVER, P. R. JAMES and J. B. JAGO), pp. 234–237. Australian Acad. Sci.

LINDSLEY D. H. and ANDERSON D. J. (1983) A two-pyroxene thermometer. *Proc. Lunar Planet. Sci. Conf. 13th*, Part 2; *J. Geophys. Res.* **88**, *Suppl.*, A887–A906.

MCCULLOCH M. T. and WASSERBURG G. J. (1978) Sm-Nd and Rb-Sr chronology of continental crust formation. *Science* **200**, 1003–1011.

MCCULLOCH M. T. and CHAPPELL B. W. (1982) Nd isotopic characteristics of S- and I-type granites. *Earth Planet. Sci. Lett.* **58**, 51–64.

MCCULLOCH M. T., ARCULUS R. J., CHAPPELL B. W. and FERGUSON J. (1982) Isotopic and geochemical studies of nodules in kimberlite have implications for the lower continental crust. *Nature* **300**, 166–169.

MCDONOUGH W. F., MCCULLOCH M. T. and SUN S.-S. (1985) Isotopic and geochemical systematics in Tertiary-Recent basalts from southeastern Australia and implications for the evolution of the sub-continental lithosphere. *Geochim. Cosmochim. Acta* **49**, 2051–2068.

MCINTYRE G. A., BROOKS C., COMPSTON W. and TUREK A. (1966) The statistical assessment of Rb-Sr isochrons. *J. Geophys. Res.* **71**, 5459–5468.

MENZIES M. A., LEEMAN W. P. and HAWKESWORTH C. J. (1983) Isotope geochemistry of Cenozoic volcanic rocks reveals mantle heterogeneity below western USA. *Nature* **303**, 205–209.

MENZIES M. A., LEEMAN W. P. and HAWKESWORTH C. J. (1984) Geochemical and isotopic evidence for the origin of continental flood basalts with particular reference to the Snake River Plain Idaho, USA. *Phil. Trans. Roy. Soc. London* **A310**, 643–660.

MORSE S. A. (1980) Kiglapait geochemistry III: Potassium and rubidium. *Geochim. Cosmochim. Acta* **45**, 163–180.

NORRISH K. and CHAPPELL B. W. (1977) X-ray fluorescence spectrometry. In *Physical Methods in Determinative Mineralogy* (ed. J. ZUSSMAN), pp. 201–272. Academic Press, London.

NWE Y. Y. (1976) Electron-probe studies of the earlier pyroxenes and olivines from the Skaergaard intrusion, east Greenland. *Contrib. Mineral. Petrol.* **55**, 105–126.

O'NIONS R. K., HAMILTON P. J. and EVENSEN N. M. (1977)

Variations in $^{143}Nd/^{144}Nd$ and $^{87}Sr/^{86}Sr$ ratios in oceanic basalts. *Earth Planet. Sci. Lett.* **34**, 13–22.

PALACZ Z. A. and TAIT S. R. (1985) Isotopic and geochemical investigation of unit 10 from the eastern layered series of the Rhum intrusion, northwest Scotland. *Geol. Mag.* **122**, 485–490.

PHILPOTTS J. A. and SCHNETZLER C. C. (1970) Phenocryst-matrix partition coefficients for K, Rb, Sr and Ba, with applications to anorthosite and basalt genesis. *Geochim. Cosmochim. Acta* **34**, 307–322.

REED S. J. B. and WARE N. G. (1973) Quantitative electron microprobe analysis using a lithium drifted silicon detector. *X-ray Spectrom.* **2**, 69–74.

ROEDER P. L. and EMSLIE R. F. (1970) Olivine-liquid equilibrium. *Contrib. Mineral. Petrol.* **29**, 275–289.

ROGERS N. W. and HAWKESWORTH C. J. (1982) Proterozoic age and cumulate origin for granulite xenoliths, Lesotho. *Nature* **299**, 409–413.

RUDNICK R. L. and TAYLOR S. R. (1986) Petrology and geochemistry of lower crustal xenoliths from northern Queensland and inferences on lower crustal composition. *Geol. Soc. Aust. Spec. Pub.* (in press).

SCHNETZLER C. C. and PHILPOTTS J. A. (1970) Partition coefficients of rare-earth elements between igneous matrix material and rock-forming mineral phenocrysts—II. *Geochim. Cosmochim. Acta* **34**, 331–340.

SHIEH Y.-N. and SCHWARCZ H. P. (1974) Oxygen isotope studies of granite and migmatite, Grenville province of Ontario, Canada. *Geochim. Cosmochim. Acta* **38**, 21–45.

STEPHENSON P. J. and GRIFFIN T. J. (1976) Cainozoic volcanicity north Queensland. Excursion Guide No. 7A, 25th International Geological Congress.

STEPHENSON P. J., GRIFFIN T. J. and SUTHERLAND F. L. (1980) Cainozoic volcanism in Northeastern Australia. In *The Geology and Geophysics of Northeastern Australia* (eds. R. A. HENDERSON and P. J. STEPHENSON), pp. 349–374. Geol. Soc. Australia, Queensland Div.

STEPHENSON R. and LAMBECK K. (1985) Erosion-isostatic rebound models for uplift: an application to south-eastern Australia. *Geophys. J. Roy. Astr. Soc.* **82**, 31–55.

STOSCH H.-G., LUGMAIR G. W. and SECK H. A. (1986) Geochemistry of granulite facies lower crustal xenoliths: implications for the geological history of the lower continental crust underneath the Eifel, West Germany. *J. Geol. Soc. Lond.* (in press).

SUN S.-S. and HANSON G. N. (1975) Origin of Ross Island basanitoids and limitations upon the heterogeneity of mantle sources for alkali basalts and nephelinites. *Contrib. Mineral. Petrol.* **52**, 77–106.

SUTHERLAND F. L. (1983) Timing, trace and origin of basaltic migration in eastern Australia. *Nature* **305**, 123–126.

TAYLOR H. P. (1980) The effects of assimilation of country rocks by magmas on $^{18}O/^{16}O$ and $^{87}Sr/^{86}Sr$ systematics in igneous rocks. *Earth Planet. Sci. Lett.* **47**, 243–254.

TAYLOR S. R. and GORTON M. P. (1977) Geochemical application of spark source mass spectrography—III. Element sensitivity, precision and accuracy. *Geochim. Cosmochim. Acta* **41**, 1375–1380.

TAYLOR S. R. and MCLENNAN S. M. (1985) *The Continental Crust: its Composition and Evolution*. Blackwell Sci. Pub., Oxford, 312p.

VALLEY J. W. and O'NEIL R. (1984) Fluid heterogeneity during granulite facies metamorphism in the Adirondacks: stable isotope evidence. *Contrib. Mineral. Petrol.* **85**, 158–173.

WASS S. Y. and HOLLIS J. D. (1983) Crustal growth in south-eastern Australia—evidence from lower crustal eclogitic and granulitic xenoliths. *J. Meta. Geol.* **1**, 25–45.

WASSERBURG G. J., JACOBSEN S. B., DEPAOLO D. J., MCCULLOCH M. T. and WEN T. (1981) Precise determination of Sm/Nd ratios, Sm and Nd isotopic abundances in standard solutions. *Geochim. Cosmochim. Acta* **45**, 2311–2323.

WELLMAN P. and MCDOUGALL I. (1974) Cainozoic igneous activity in eastern Australia. *Tectonophys.* **23**, 49–65.

WELLS P. R. A. (1977) Pyroxene thermometry in simple and complex systems. *Contrib. Mineral. Petrol.* **62**, 129–139.

WHITE W. M. and HOFMANN A. W. (1982) Sr and Nd isotope geochemistry of oceanic basalts and mantle evolution. *Nature* **296**, 821–825.

WILKINSON J. F. G. and TAYLOR S. R. (1980) Trace element fractionation trends of tholeiitic magma at moderate pressure: evidence from an Al-spinel ultramafic-mafic inclusion suite. *Contrib. Mineral. Petrol.* **75**, 225–233.

WILSON A. F. and BAKSI A. K. (1983) Widespread ^{18}O depletion in some Precambrian granulites of Australia. *Precamb. Res.* **23**, 33–56.

WILSON J. R. and LARSEN S. B. (1985) Two-dimensional study of a layered intrusion—the Hyllingen Series, Norway. *Geol. Mag.* **122**, 97–124.

WITHNALL I. W. (1982) The geology of the Greenvale-Baicooma area. In *1982 Field Conference, Charters Towers-Greenvale Area* (ed. I. W. WITHNALL), pp. 31–46. Geol. Soc. Australia, Queensland Division.

APPENDIX

PETROGRAPHIC DESCRIPTIONS OF ANALYZED SAMPLES

Plagioclase-rich samples

83-107. Polygonal, optically zoned labradorite forms medium-grained (~0.3 mm) matrix around larger (up to 4 mm) deformed plagioclase (labradorite) with irregular grain boundaries, and elongate olivine-centered coronas. Olivine (Fo_{54-70}, variably altered to red-brown iddingsite) is rimmed by orthopyroxene which is generally rimmed by fine-grained spinel-pyroxene symplectite. Rare, large (~4 mm), optically continuous, poikilitic orthopyroxenes show some exsolution lamellae. Plagioclase within orthopyroxene have preserved lath-shaped crystal form. Plagioclase contains tiny (~5–10 μm), euhedral spinel inclusions.

83-112. Medium-grained (~0.5 mm), polygonal andesine matrix surrounds clusters of polygonal clinopyroxene (with thin exsolution lamellae)-orthopyroxene-magnetite (with ilmenite exsolution). Magnetite/ilmenite rimmed by dark alteration rims. Oriented oxide inclusions within clinopyroxene. Plagioclase devoid of spinel inclusions. Grain boundaries altered.

83-114. Medium-grained (~1.5 mm), zoned, deformed and broken labradorite (with andesine rims) with irregular grain boundaries surrounds irregularly-shaped, zoned and fractured clinopyroxene and orthopyroxene crystals and symplectic spinel-pyroxene intergrowths. Garnet forms completely kelyphitized thin rims around spinel. Grain boundaries altered. Plagioclase contains small (~75 μm), elongate spinel inclusions.

83-117. Medium-grained (0.6 mm), polygonal andesine surrounds symplectic intergrowths of pyroxene-spinel. Spinel surrounded by completely kelyphitized garnet. Orthopyroxene altered yellowish-brown with dark brown staining in fractures, some spinel altered to lemon yellow color. Much grain-boundary alteration. No spinel inclusions within plagioclases.

83-125. Coarse- to medium-grained (4 to 0.5 mm) andesine (large grains broken, small grains polygonal) forms matrix around euhedral garnet and garnet-clinopyroxene intergrowths or clusters. Clinopyroxene has typically smooth grain boundaries and no exsolution lamellae. Orthopyroxene rare. Rare, small (~250 μm) spinel cores occur at center of euhedral garnets. Garnets totally kelyphitized. Grain boundaries and fractures altered. Plagioclase devoid of spinel inclusions.

83-127. Coarse-grained (up to 3 mm), zoned, fractured labradorite, with andesine rims, surrounds clusters of clinopyroxene and coarse-grained symplectic orthopyroxene-spinel, which are sometimes rimmed by clinopyroxene. Plagioclase contains large (~150 μm), euhedral spinel inclusions.

83-131. Coarse-grained (up to 4 mm), zoned, deformed labradorite crystals (with andesine rims) form irregular grain boundaries with large (~2 mm) clinopyroxene crystals which show abundant exsolution lamellae. Smaller (~0.3 mm), polygonal clinopyroxenes have no exsolution. Euhedral garnet found within plagioclase matrix. Symplectic pyroxene-garnet rimmed by orthopyroxene. Some relict spinels at center of symplectic pyroxene-garnet intergrowths. Clinopyroxene rims orthopyroxene. Rare secondary amphibole. Some plagioclase crystals contain large (~150 μm), euhedral spinel inclusions. Grain boundaries relatively free of alteration.

83-133. Medium-grained (~0.5 mm), polygonal andesine forms matrix around mosaic-textured clinopyroxene clusters, symplectically intergrown orthopyroxene-garnet, and euhedral garnet. Occasional spinel cores at center of symplectites; no spinel observed at centers of euhedral garnets. Garnet within symplectite and garnet rims all kelyphitic. Some plagioclase crystals riddled with small (~30 μm), euhedral spinel inclusions. Grain boundaries have thin coating of brown material.

83-138. Coarse-grained (up to 4 mm), zoned, deformed and broken labradorite crystals with irregular grain boundaries form matrix around large (~5 mm) clusters of coarse-grained (up to 4 mm) clinopyroxene with smaller orthopyroxene and spinel. Coarse-grained clinopyroxene shows abundant thin exsolution lamellae and contains many CO_2-rich fluid inclusions. Spinel symplectically intergrown with pyroxene. Spinels sometimes have very thin, kelyphitized garnet rims. Orthopyroxene tends to be concentrated toward outside of clusters or within plagioclase matrix. Grain boundaries and fractures altered. Plagioclase does not contain euhedral spinel; some large clinopyroxenes contain spinel inclusions.

83-140. Coarse-grained (up to 4 mm), deformed and broken labradorite (rimmed by andesine), surround garnet-pyroxene symplectites and large, deformed clinopyroxenes and orthopyroxenes with exsolution lamellae. Rare spinel at center of garnet/pyroxene intergrowths. Orthopyroxenes rimmed by clinopyroxene when in contact with plagioclase. Some orthopyroxenes contain needle-like inclusions of rutile(?). Garnet heavily kelyphitized leaving only unaltered cores. Minor, small, red-brown amphibole. Rare ilmenite and zircons (<16 μm long). Grain boundaries altered. Plagioclase contains ~150 μm long spinel inclusions.

Pyroxene-rich samples

83-110. Coarse-grained (up to 3 mm), polygonal to irregular labradorite crystals with smaller, oval clinopyroxene and orthopyroxene crystals interlayered with coarse-grained clinopyroxene-orthopyroxene layers with minor plagioclase and rutile. Some of the larger pyroxene crystals have exsolution lamellae in two directions. Grain boundaries altered. Plagioclase does not contain spinel inclusions.

83-115. Coarse-grained (up to 4 mm), polygonal to irregular clinopyroxene and smaller orthopyroxene predominate with interstitial labradorite and rutile. Rare, thin exsolution lamellae in clinopyroxenes. Opaques occur along grain boundaries. Small rutile inclusions within pyroxenes. Plagioclase devoid of spinel inclusions.

Transitional samples

83-126. Coarse-grained (up to 3 mm), zoned, deformed labradorite, with andesine rims and irregular grain boundaries occurs with large (up to 3 mm) clinopyroxenes (with abundant exsolution lamellae) and orthopyroxenes. Clinopyroxene contains rutile lamellae. Spinel is intergrown with orthopyroxene and rimmed by clinopyroxene. Spinel and orthopyroxene rims altered dark brown. Grain boundaries and fractures altered and iron-stained. Plagioclase contains rare spinel inclusions.

BC. Medium-grained (~0.3 mm), generally untwinned, polygonal andesine crystals occur with euhedral garnets and large (up to 4 mm), recrystallized clinopyroxenes which often have an irregularly distributed, peculiar, vermicular-like texture. Rare, pale green spinels at center of some garnets. Garnets completely kelyphitized. Pyroxenes contain very small (~70 μm), irregular, pleochroic (biotite?) and opaque inclusions. Plagioclase devoid of spinel inclusions.